Chapter 3. High-Frequency (>100 GHz) and High-Speed (<10 ps) Devices

Academic and Research Staff

Professor Qing Hu, Dr. Gerhard de Lange

Visiting Scientists and Research Affiliates

Dr. Simon Verghese

Graduate Students

Erik K. Duerr, Kostantinas Konistis, Ilya Lyubomirsky, Arifur Rahman, Farhan Rana, Brian P. Riely, Ben S. Williams, Bin Xu, Noah D. Zamdmer

3.1 Introduction

The millimeter-wave and THz frequency (f > 100 GHz) range remains one of the most underdeveloped frequency ranges, even though there are a great number of potential applications in remote sensing, spectroscopy, plasma diagnostics, and communications. This is because the millimeter wave and far-infrared frequency range falls between two other frequency ranges, the microwave frequency range and the near-infrared and optical frequency range, in which conventional semiconductor devices are usually operated.

Semiconductor devices, which utilize the classical diffusive transport of electrons, such as diodes and transistors, have a high frequency limit. This limit is set by the time it takes for electrons to travel a certain distance. Currently, electron mobility and the smallest feature size which can be fabricated by lithography limit the frequency range to below several hundred GHz. Semiconductor devices based on quantum mechanical interband transitions, however, are limited to frequencies higher than those corresponding to the semiconductor energy gap, which is higher than 10 THz for most bulk semiconductors. Therefore, a large gap exists from 100 GHz to 10 THz in which very few devices are available.

Semiconductor quantum-effect devices (which can be loosely termed "artificial atoms"), including both vertically grown quantum-well structures and laterally confined mesoscopic devices, are human-made quantum mechanical systems in which the energy levels can be chosen by changing the sizes of the devices. Typically, the frequency corresponding to the intersubband transitions is in the millimeter-wave to THz range ($\Delta E \sim$ 1-4 meV) for the lateral quantum-effective devices and above one THz for the vertical quantum wells. It is therefore appealing to develop ultrahigh-frequency devices, such as radiation detectors and mixers, and THz lasers utilizing the intersubband transitions in these devices. Furthermore, the study of the interaction between photons (with energies comparable to the intersubband spacings) and the quantum-effect devices (artificial atoms) is analogous to optical spectroscopy in atomic physics. Naturally, this study will literally shine "new light" on these novel devices and new information can be obtained that cannot be extracted from dc transport measurements. It is also clear that devices with THz characteristic frequencies will have picosecond speed response. Such ultrahigh-speed devices could be useful in easing the electronic "bottleneck" in the current fiber optical communication systems, in which only a small fraction of the 20-THz bandwidth of optical fibers are utilized because of the slow speed of electronic devices.

In addition to new physical concepts, novel technologies must also be developed to meet the challenges at these high frequencies. Conventional mechanically machined horn antennas integrated with waveguide cavities have been the workhorse at microwave and millimeter-wave frequencies since they were first implemented more than fifty years ago during World War II. Very high antenna gain and essentially perfect antenna efficiency can be achieved using these structures. However, they are expensive, bulky, and incompatible with arrays. In order to overcome these problems, progress has been made in using micromachining to fabricate the horn antenna structures. In these structures, the active elements and their planar antennas are fabricated on a free-standing thin (~1 micron) SiN membrane, which is suspended over a silicon pyramidal horn that is formed by anisotropic etching, or micromachining. The side walls of this micromachined

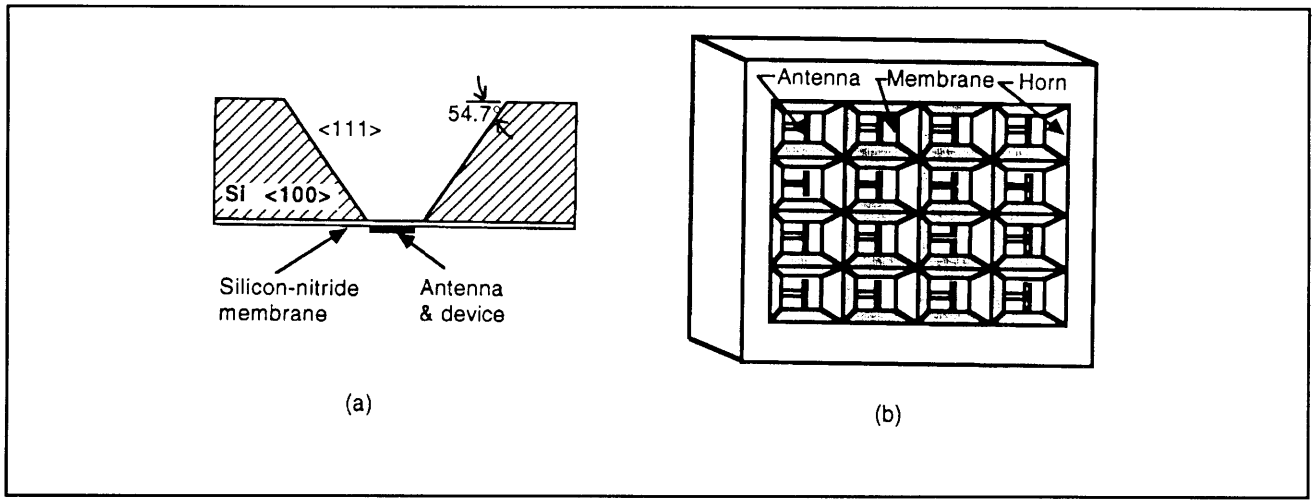

Figure 1. (a) Example of a micromachined horn antenna structure that is made by anisotropically etching a <100> silicon wafer. (b) Schematic of a focal-plane array on a single wafer made using micromachining.

structure can then be coated with Au to form a horn antenna. Compared to conventional waveguide horn antennas, this novel micromachined structure has several major advantages. It is easier to fabricate fine three-dimensional structures by using photolithography. A horn antenna with micron precision can be easily defined and inexpensively mass produced. It is made on Si or GaAs wafers compatible with thin-film technology. Thus, active elements, such as RF and IF amplifiers, mixers and video detectors, local oscillators, and post-detection signal processors, can be integrated monolithically with the antenna's structure to form monolithic transmitter/receiver systems. The antenna is lightweight and compact. The most attractive feature of the micromachined structure is that focal-plane arrays can be fabricated easily on a single wafer, as illustrated in figure 1b. Such systems will yield a significantly improved spatial resolution in remote sensing, and a much greater antenna gain when implemented with phased-arrays. In our group, we are systematically investigating physical and engineering issues that are relevant to high-frequency and high-speed devices. Specifically, we are working on micromachined millimeter- and submillimeter-wave devices, far-infrared and picosecond time-resolved transport studies of lateral quantum-effect devices, and development of far-infrared lasers, photodetectors, and optical parametric amplifiers using multiple quantum-well structures.

3.2 Micromachined Millimeter-wave Devices

Sponsors

National Aeronautics and Space Administration
Grant NAGW-4691
National Science Foundation
Grant AST 94-23608
U.S. Army Research Laboratory/Federated Laboratory
Grant QK-8819

Project Staff

Dr. Gerhard de Lange, Arifur Rahman, Erik K. Duerr, Kostantinas Konistis, Professor Qing Hu, in collaboration with Dr. Gerry Sollner,[1] Dr. Arthur Lichtenberger,[2] Dr. Ray Robertazzi[3]

3.2.1 Micromachined Millimeter-wave SIS Receivers

SIS (superconductor-insulator-superconductor) heterodyne receivers have been demonstrated to be the most sensitive receivers throughout 30-840 GHz frequency range. The challenge now in the SIS receiver technology is to extend their operating fre-

[1] Group 86 at MIT Lincoln Laboratory, Lexington, Massachusetts.

[2] University of Virginia, Charlottesville, Virginia.

[3] Hypres Inc., Elmsford, New York.

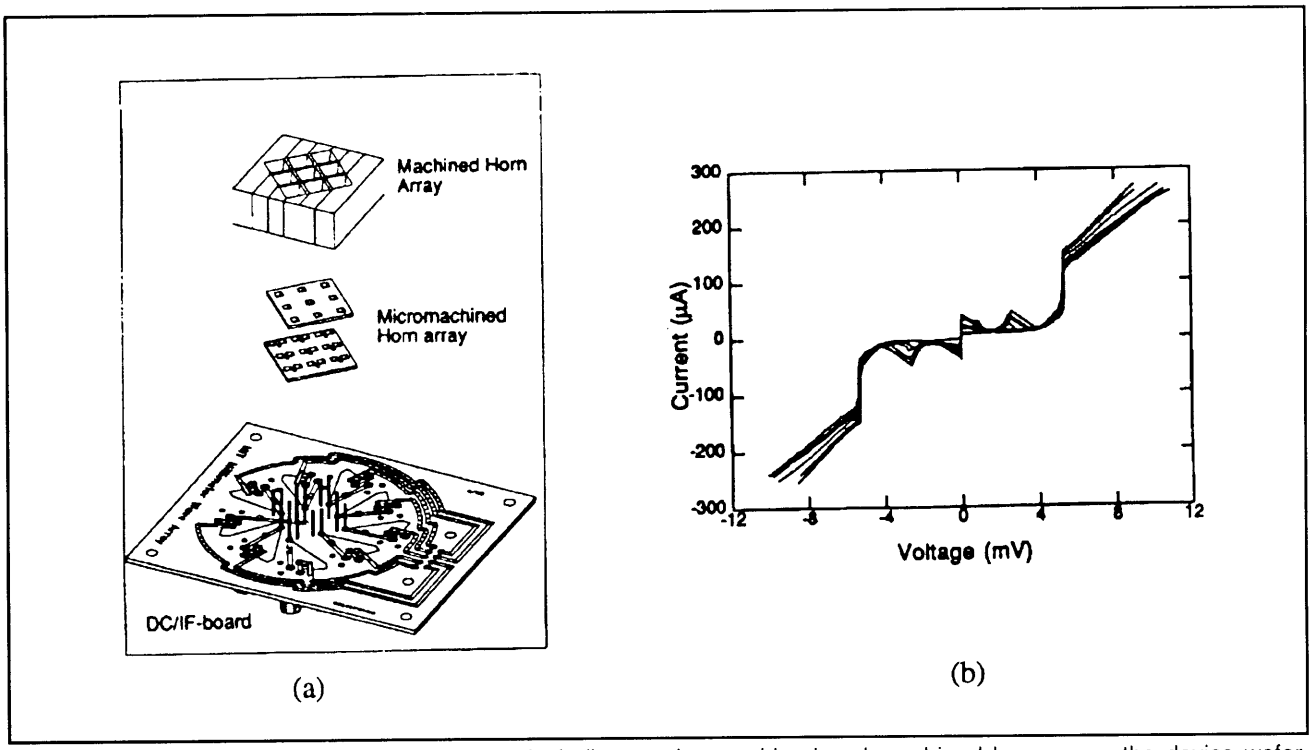

Figure 2. (a) Schematic of an array structure including a micromachined and machined horn array, the device wafer, and the dc and IF connection board. (b) I-V curves of seven SIS junctions in the array.

quency into the THz range and to develop focal-plane arrays to improve the efficiency of data acquisition. In order to achieve these goals, we are currently developing a novel scheme to couple the millimeter-wave and infrared signals to the superconducting devices by using a micromachined horn antenna and a planar antenna supported by a thin (~1 micron) membrane, as shown in figure 1a. As stated in the introduction, this novel micromachined antenna structure can be produced with a high precision using photolithography, and it can be utilized in focal-plane arrays, as shown in figure 1b.

Following our recent success in developing single-element micromachined SIS receivers (see our previous publication in *Applied Physics Letters* 68: 1862 (1996), we have designed and constructed a 343 focal-plane array with the center frequency around 200 GHz. The schematic of the structure is shown in figure 2a which includes a micromachined and mechanically machined horn array, a device wafer, and a dc and IF connection board. Preliminary measurements of the dc I-V characteristics showed good uniformity across the entire array. Figure 2b shows the I-V curves from seven SIS junctions in the array. The resistance variation of these junctions is within 5 percent. We are currently in the process of measuring both the video and heterodyne response of the focal-plane array. Our next step will be to integrate on-chip Josephson-junction local oscillators with the SIS mixers to form monolithic focal-plane arrays.

3.2.2 Micromachined Room-temperature Millimeter-wave Sensors

Due to (1) the penetration capability of a millimeter wave (especially around the 94-GHz atmospheric window) in foggy, dusty, and smoky environments, and (2) its better spatial resolutions compared to the longer wavelengths at microwave frequencies, sensitive room-temperature millimeter-wave devices are very useful in imaging,and in object identification and tracking. These devices are important for both military and commercial applications, such as motor vehicle collision avoidance radars. Based on our recent remarkable success in the development of micromachined SIS receivers, we are currently developing the most sensitive room-temperature millimeter-wave sensors using the micromachining technology.

We have used microbolometers (whose dimensions are approximately several microns, as shown in figure 3) in our micromachined systems. Microbolometers are easy to make (in fact, they are much easier to make than the superconducting tunnel junctions in our current systems), robust, and sensitive. In addition, our micromachined millimeter-wave structure is ideal for bolometric detectors in

such a way that the thin SiN membrane provides a natural thermal isolation that a sensitive bolometer requires.

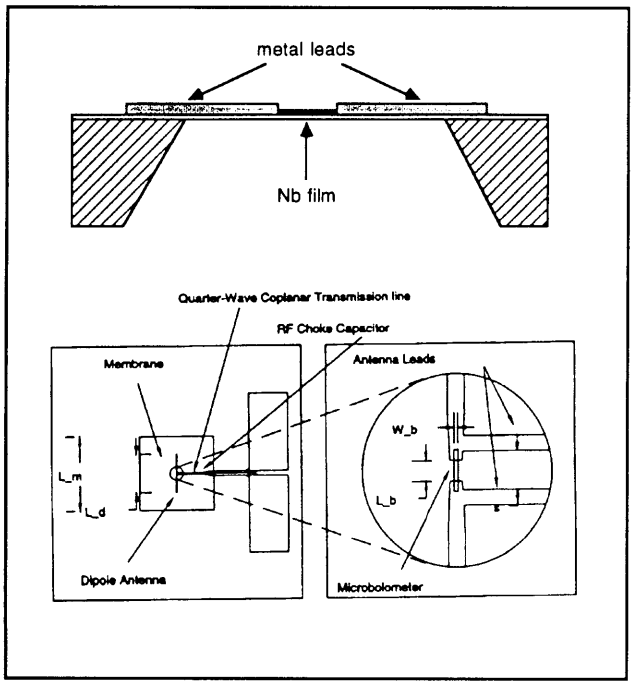

Figure 3. Schematic of a microbolometer supported by a thin membrane, which provides a good thermal insulation. The lower figures are top views of the antenna-coupled microbolometers.

The dominating noise source in bolometric detectors is the 1/f noise associate with the resistive element, which is usually made out of semimetal materials, such as Bi, to achieve a high resistance value for impedance matching. Recently in the field of superconducting electronics, it was discovered that a commonly used superconducting material, Nb, has an order of magnitude level of 1/f noise (at room-temperature) that is lower than Bi while still provides sufficiently high resistivity for impedance matching. Assume we operate the microbolometers above the 1/f noise frequency region and use low-noise on-chip amplifiers, the NEP (noise equivalent power) of the microbolometers is limited by the temperature fluctuation, i.e., the phonon noise. Using realistic parameters for thermal conductance, a room-temperature Nb microbolometer can achieve an NEP of 6×10^{-12} W/(Hz)$^{1/2}$. This is more than one order of magnitude lower than that of pyroelectric detectors, which are the commonly used room-temperature millimeter-wave sensors. This level of reduction in NEP will significantly improve the sensitivity of the detectors and reduce the required integration time by at least a factor of one hundred for the same signal/noise ratio.

3.3 Far-infrared and Picosecond Time-resolved Transport Studies of Quantum-effect Devices

Sponsor

National Science Foundation/MRSEC
Grant DMR 94-00334

Project Staff

Dr. Simon Verghese, Noah D. Zamdmer, Farhan Rana, Arif Rahman, Professor Qing Hu, in collaboration with Dr. Michael R. Melloch,[4] Dr. Michael J. Rooks[5]

Quantum transport has been one of the most active fields in solid-state physics in recent years. Advances in material preparation have made quantum phenomena profound in electron transport for many semiconductor quantum devices such as quantum point contacts, quantum dots, quantum wires, quantum wells, superlattices, etc. In clean samples and at low temperatures, electrons can travel through the whole sample without suffering phase-destructive scattering. Extensive work has been done to study various features of such phase-coherent quantum transport. However, most of the experiments reported so far are limited to dc transport measurements and far-infrared spectroscopy measurements.

It is well known in the field of superconducting tunneling that photons can assist the tunneling process, provided the tunneling is elastic. In a broad sense, elastic tunneling is a phase-coherent quantum transport process in a classically forbidden region. Therefore, all the results of photon-assisted tunneling can be applied to the study of photon-assisted quantum transport in semiconductor devices. This will provide a new dimension to study the exciting quantum transport phenomena. Novel long-wavelength optoelectronic devices may also emerge from this research.

In this project, we have performed extensive studies on antenna-coupled lateral quantum-effect devices

[4] Purdue University, West Lafayette, Indiana.

[5] Cornell National Nanofabrication Facility, Cornell University, Ithaca, New York.

under irradiation at millimeter-wave and THz frequencies. The motivation for this investigation is two-fold. First, studying the response of quantum-effect devices (or artificial atoms) to radiation at frequencies comparable to the intersubband spacings is analogous to optical spectroscopy in atomic physics. Therefore, new information can be revealed through this type of study that otherwise dc-transport measurement alone may not reveal. Secondly, the intrinsically lower capacitance (and therefore, the time constant RC) of laterally confined quantum-effect devices should make them competitive candidates for application at and above one THz, where no photonic devices are currently available.

We first investigated the simplest quantum-effect device, quantum point contact (QPC), which is simply a split-gate field-effect transistor. The electron transport from the source to drain can be modeled by a one-dimensional quantum mechanical system with a barrier at the narrowest constriction. Under far-infrared irradiation, whose photon energy is sufficient to raise the electron energy over the barrier, a radiation-induced drain/source current should be produced that is directly analogous to the photoemission phenomenon in metals. Despite the intuitively plausible picture and the straightforward analogy with photoemission phenomenon, our experimental investigations have yielded only bolometric signals. In order to understand why such a well-established photon-assisted process in many other systems has not been observed in QPCs, we have performed simulation studies by numerically solving the time-dependent Schrödinger equation. Our main finding is that the selection rule, which is the mathematical statement of the momentum conservation of the electron/photon systems, forbids transitions between two spatially extended electron states. Mathematically, in order to achieve an appreciable photon-excited transition probability, the dipole-moment integration must be truncated to a region that is not much greater than the inverse of the momentum difference between the initial and final electron states. This can be achieved experimentally by either a localized electron state or a localized photon-field profile. Physically, this spatial localization provides the momentum spread necessary for momentum conservation in the photon excitation process.

Based on this understanding, we have designed and fabricated lateral quantum-well structures with dual-gate electrodes. The localized nature of the quasibound states in the quantum well ensures that the selection rule can be satisfied. Experimentally, the radiation-induced currents at 90 GHz and 270 GHz exhibit distinctly different features. This frequency-dependent behavior is evidence that the radiation-induced current is a result of photonic effect that depends on the energy of individual photons. By modeling the photon-assisted transport process using an effective transmission coefficient, which is a superposition of the original transmission coefficient shifted by the photon energy, we have calculated photon-induced current that agrees well with the experimental results.

Although our work in frequency domain has yielded new information about quantum-effect devices, a complementary approach is to study the response of the quantum devices in time-resolved fashion by using a pump-and-probe method with a pulsed laser. A 100-fs laser pulse contains frequency components up to 10 THz, which should enable us to perform spectroscopic studies on quantum devices over a broad frequency range that covers all the interesting energy levels, namely the intersubband transition and Coulomb interaction energies. Furthermore (and perhaps the most attractive feature of the time-domain studies), the time-resolved studies can reveal information that frequency-domain studies cannot reveal, namely the time scale of transport process in quantum devices. This is one of the basic issues in determining the potential applications of the quantum devices.

We are pursuing two types of measurements in this project. The first one involves a far-infrared spectrometer pumped by a mode-locked Ti:Sapphire laser which we have constructed recently, as shown in figure 4. In this set up, two antenna-coupled Auston switches are pumped by a $Ti:Al_2O_3$ pulsed laser. The THz electrical pulses are launched into free space and then combined by a beam splitter. The combined beam is a superposition of two coherent subpicosecond electrical pulses whose relative time delay can be varied. These combined pulses will then be focused onto an antenna-coupled quantum device and generate a dc electrical current in the device through the photon-assisted transport/tunneling process. Effectively, the generated electrical current is proportional to the time autocorrelation function of the whole system, whose Fourier transform will give the frequency response of the system. This measurement is essentially the same as that using a conventional far-infrared Fourier transform spectrometer (FTS), which uses a Hg-arc lamp as its source. There are several major advantages of the pulsed laser system, however. First, its source is much brighter than that of the FTS so that far-infrared nonlinear spectroscopy can be performed. Second, the short duration of the laser pulses minimizes the heating effect and thus enhances the relative strength of the photon-assisted quantum process.

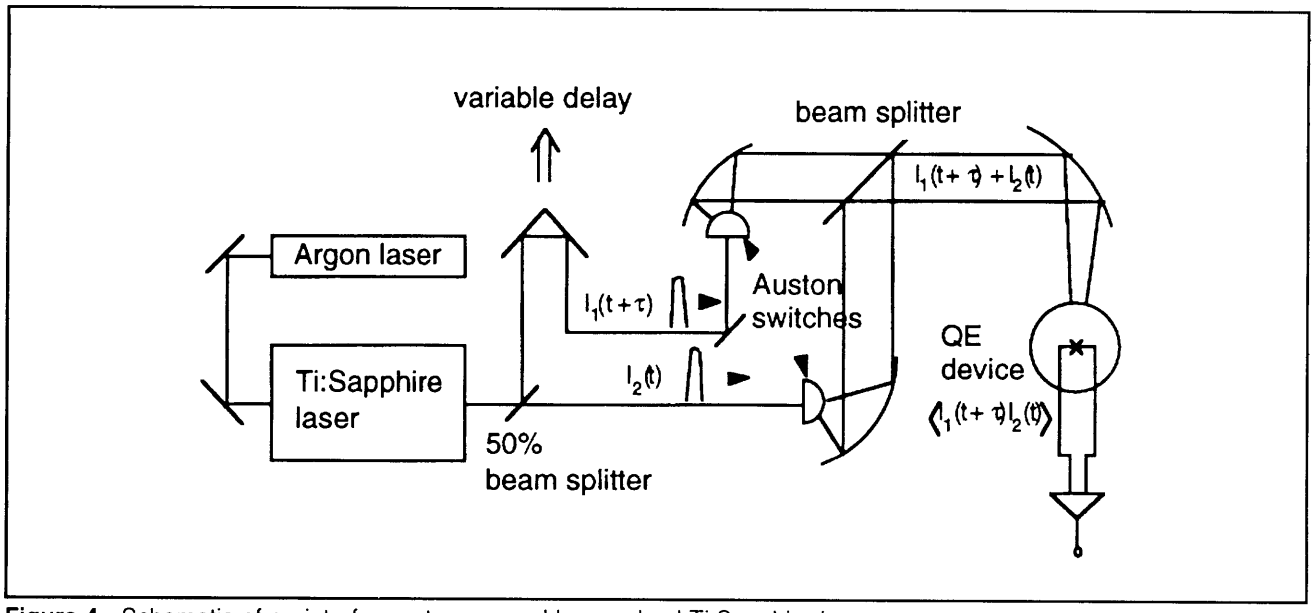

Figure 4. Schematic of an interferometer pumped by a pulsed Ti:Sapphire laser.

The second type of experiment involves a pump-and-probe method, by integrating two Auston switches *monolithically* with the quantum-effect devices, as shown in figure 5. One switch will be used to apply a short electric pulse on the input, and the second one will be used to probe the output electrical current in a time-resolved fashion. This scheme differs from the first one in that the pump and probe beams are focused on *different* spots. In this way, we can measure the time scale of the transport process from the input to the output, as well as the spectroscopic information of the system. In order to achieve a high speed from the Auston switches, lattice-matched low-temperature-grown (LTG) GaAs materials will be used which have subpicosecond recombination time.

In order to pursue the time-resolved pump-and-probe measurements on quantum-effect devices, we have constructed a cryostat with optical fiber couplers that can bring sub-picosecond laser pulses to the cryogenic stage. The schematic of the system is shown in figure 6, along with the schematic of coplanar transmission lines that provide the dc biases of the pump and probe Austin switches and the propagation path for the generated picosecond electrical pulses.

Figure 7 shows the pump-and-probe measurements performed at (a) 300 K, (b) 77 K , and (c) 4.2 K. The system clearly works well at cryogenic temperatures. In comparison, the insert plots the pump-and-probe measurement performed in the free space. The broadened pulses in the fiber-coupled

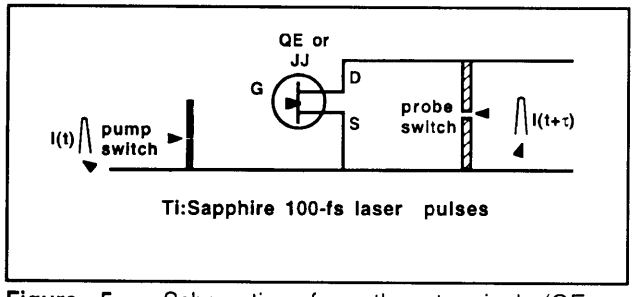

Figure 5. Schematic of a three-terminal (QE or Josephson) device pumped by a subpicosecond electrical pulse at the input. The induced output current can be time-resolved by another time-delayed probe beam.

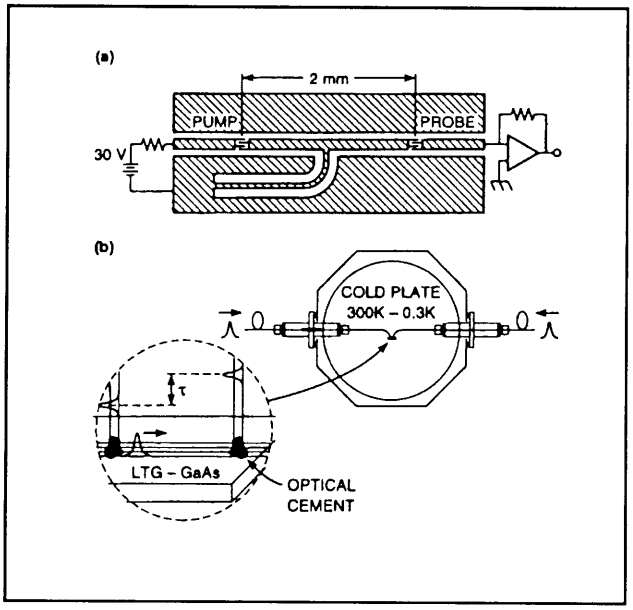

Figure 6. (a) Two Austin switches coupled through a coplanar transmission line. (b) Schematic of a cryostat with optical fiber couplers that bring subpicosecond laser pulses to the cryogenic stage.

experiments is due to the fiber dispersion of the 100-fs pulses. In future experiments, we will use the picosecond mode of our laser. Counterintuitively, laser pulses of picosecond width suffer much less dispersion while traveling through the fibers, and therefore will result in shorter pulses at the end.

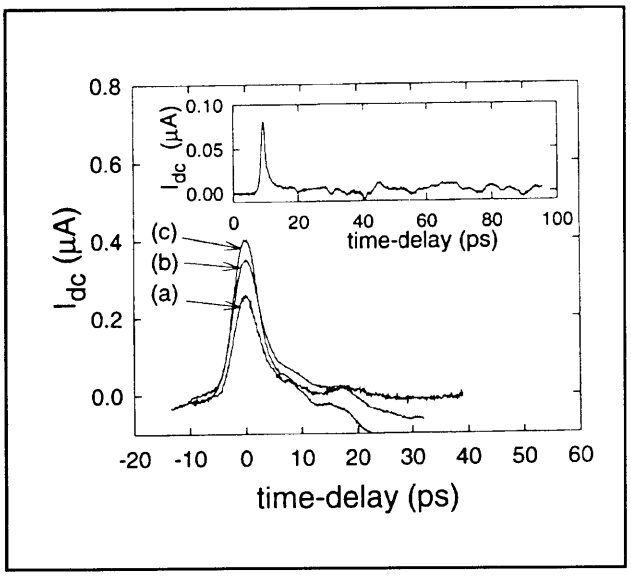

Figure 7. Insert: pump-and-probe results for the transmission line with free-space coupled optical beams. Main figure: results measured using the fiber coupled cryostat, (a) at 300 K, (b) at 77 K, and (c) at 4.2 K.

3.4 Intersubband-transitions Lasers and Optical Parametric Oscillators

3.4.1 THz Lasers Using Multiple Quantum-well Structures

Sponsor

U.S. Army Research Office
Grant DAAH04-95-1-0610
Federated Laboratory
Grant QK-8819

Project Staff

Bin Xu, Brian P. Riely, Ben S. Williams, Professor Qing Hu, in collaboration with Dr. Michael R. Melloch[6]

Semiconductor quantum wells are human-made quantum mechanical systems in which the energy levels can be designed and engineered to be of any value. Consequently, unipolar lasers based on intersubband transitions (electrons that make lasing transitions between subband levels within the conduction band) were proposed for long-wavelength sources as early as the 1970s. However, because of the great challenge in epitaxial material growth and unfavorable fast nonradiative relaxation rate, unipolar intersubband-transition lasers (also called quantum-cascade lasers) at near-infrared (4-5 μm) and mid-infrared (8-11 μm) wavelengths were developed only recently at Bell Laboratories.

This achievement is remarkable, but the technique used in the original quantum-cascade lasers will not be directly applicable for the longer-wavelength THz range because of two major obstacles. First, the energy levels corresponding to THz frequencies (1 THz = 4 meV) are quite narrow, so the requirements for the design and fabrication of suitable quantum wells are demanding. Because of the narrow separation between subband levels, heating and hot-electron tunneling will have a much greater effect. Also, the small energy scales of THz photons make the detection and analysis of spontaneous emission (a crucial step toward developing lasers) quite difficult. Secondly, and perhaps the most important, mode confinement, which is essential for any laser oscillation, is difficult at longer wavelengths. Conventional dielectric-waveguide confinement is not applicable because the evanescent fiel penetration, which is proportional to the wavelength and on the order of several tens of microns, is much greater than the active gain medium of several microns. We are currently developing intersubband-transition lasers based on our recent success in generating and detecting THz emission signals and on a novel mode confinement method using metallic waveguide structures.

In order to provide an inverted population for lasing action, we have designed a three-level system based on a module of three quantum wells. Figure 8 shows one such module (shown as a solid line) connected in series with two other identical modules (shown as a dashed line). The conduction-band profile and the square of the electron wavefunctions were calculated numerically by solving Schrödinger and Poisson equations self-consistently. The radiative transition takes place between E_3 and E_2. The separation between E_2 and E_1 is designed to be slightly greater than the LO phonon energy $\hbar\omega_{LO}$, which is 36 meV in GaAs.

[6] Purdue University, West Lafayette, Indiana.

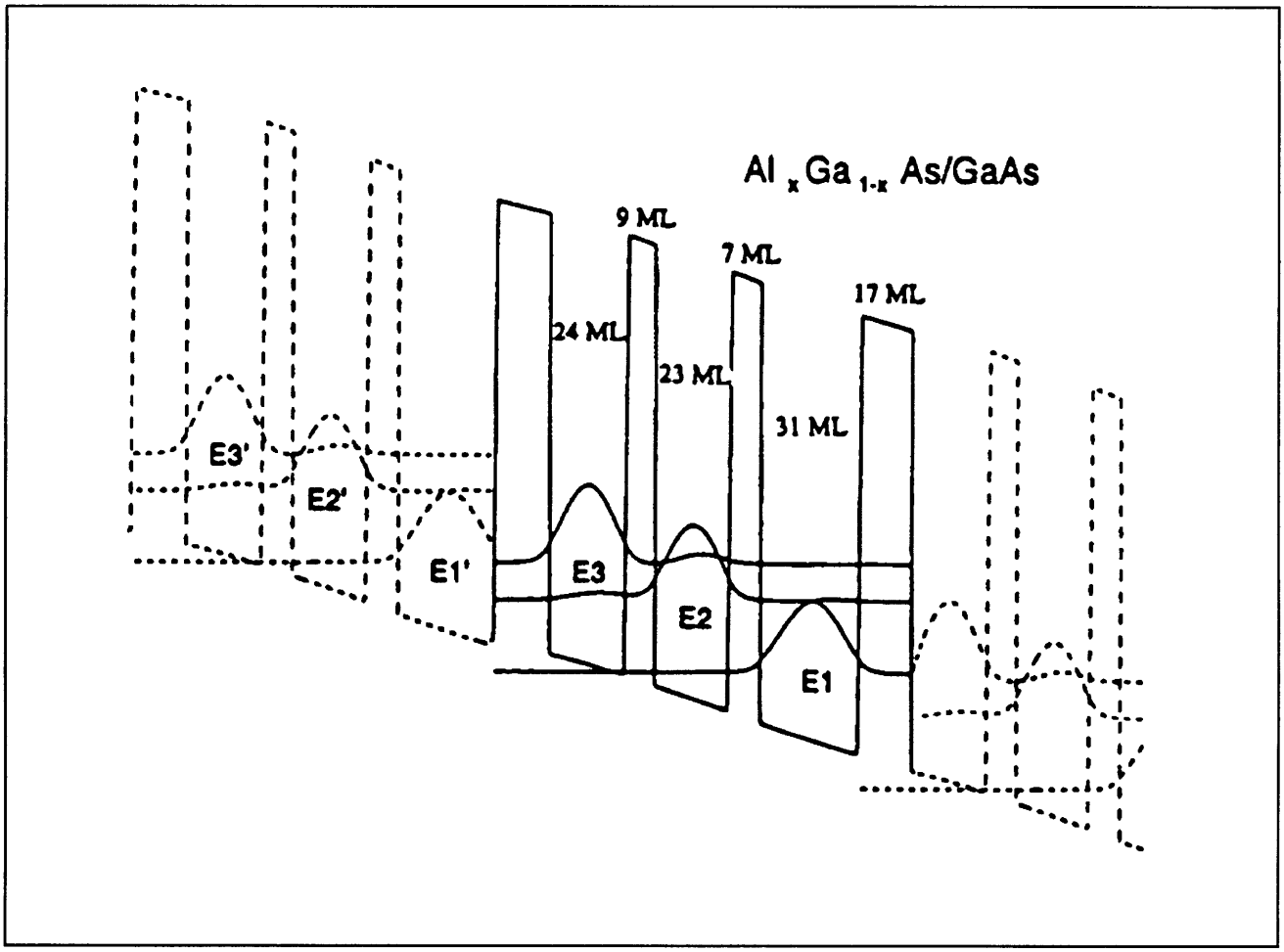

Figure 8. Schematic of a three-level system based on a triple quantum-well structure. The radiation transition takes place between E_3 and E_2, and the fast LO-phonon emission keeps the level E_2 empty. The conduction-band profile and the square of the electron wavefunctions were calculated numerically from Schrödinger and Poisson equations.

Consequently, very fast (~1 ps) LO-photon emission will keep the level E_2 empty. Transport of electrons between adjacent modules is achieved through resonant tunneling, when the ground state subband E_1' of a previous-stage module is aligned with the upper subband E_3 of the following stage, as shown in figure 8. The use of many such modules will increase the mode confinement factor. It will also reduce the rate of electron-electron scattering by lowering the three-dimensional electron density that is proportional to the inverse of the number of modules.

The current-voltage and THz power-voltage relations of one device with 10 modules of triple quantum wells are shown in figure 9. The current increases rapidly with voltage, but then saturates at $V \geq 0.7$ V. At that point we believe the ground state level E_1' is aligned with the upper level E_3 of the following module throughout the entire structure, as illustrated in figure 8. As the voltage increases beyond this point, the energy levels become misaligned and the current saturates. (We have observed negative dynamic resistance in several devices in this voltage region.) The emitted THz power (coupled out of the MQW structure through the surface by a diffraction grating) is measured using a Ga:Ge far-infrared photoconductive. As shown in figure 9b, the power increases abruptly at $V \approx 0.7$ V and saturates at $V \geq 1$ V.

Using a far-infrared measurement set-up including an external Fourier transform spectrometer, we were able to spectrally resolve the emitted far-infrared signals. The inset in figure 10 shows one of the measured interferograms, whose Fourier transform yielded the spectrum shown in the main figure. The cut-off frequency of the Ga:Ge detector was approximately 2 THz, below that the data was unreliable, and thus we truncated the spectrum at 2 THz. The center frequency of the emission spectrum is at 2.5 THz and the 3-dB linewidth is approximately 0.5 THz. The dashed line is a Lorentzian fit, whose good agreement with the measured spec-

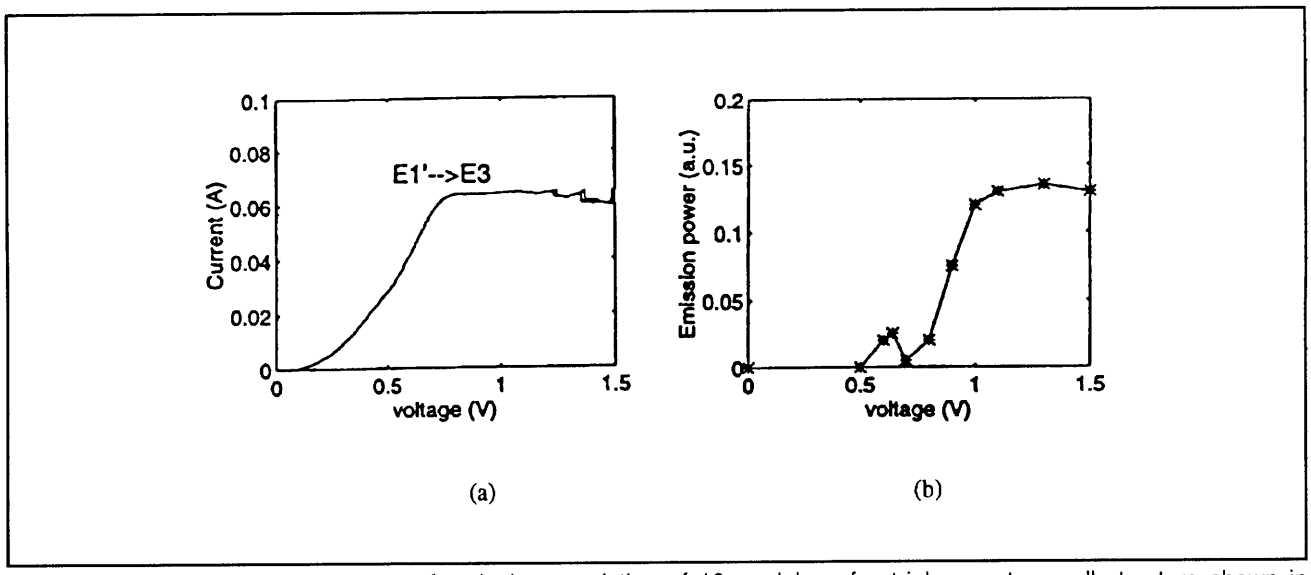

Figure 9. (a) Current-voltage curve of a device consisting of 10 modules of a triple quantum-well structure shown in figure 3. (b) Far-infrared power-voltage curve measured from the same device.

trum indicates that the linewidth is mainly determined by homogeneous broadening.

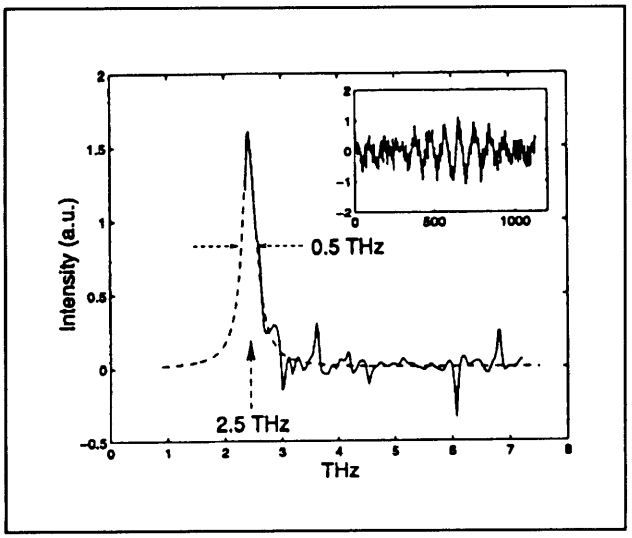

Figure 10. Spectrum of a measured THz emission from the same device described in figure 8. The center frequency is at 2.5 THz and the 3-dB linewidth is approximately 0.5 THz. The inset is the original interferogram that was measured using a Fourier transform spectrometer.

3.4.2 Far-infrared Optical Parametric Amplifiers Using DQWs

Sponsor

Hertz Foundation Fellowship
U.S. Army Research Office/AASERT
Grant DAAH04-94-G-0167

Project Staff

Ilya Lyubomirsky, Professor Qing Hu, in collaboration with Dr. Ben Streetman[7]

It is well known in the field of nonlinear optics that the nonlinear susceptibility $\chi^{(2)}$ is large near a resonant frequency for a system that lacks inversion symmetry. Such a large $\chi^{(2)}$ has been widely used in second harmonic generation, second frequency generation, and parametric amplification at optical and near-infrared frequencies, where coherent sources at pump frequencies are available. As far as its optical properties are concerned, a quantum-well device acts like a giant atom, whose resonant frequencies are in the mid- to far-infrared frequencies. Naturally, if we design a QW structure such that it has resonances at mid-infrared frequency (λ~ 10 microns) and far-infrared frequencies, we can use widely available CO_2 lasers as a pump source to parametrically generate far-infrared radiations. This nonlinear photon conversion process is illustrated in figure 11a.

[7] College of Engineering, University of Texas, Austin, Texas.

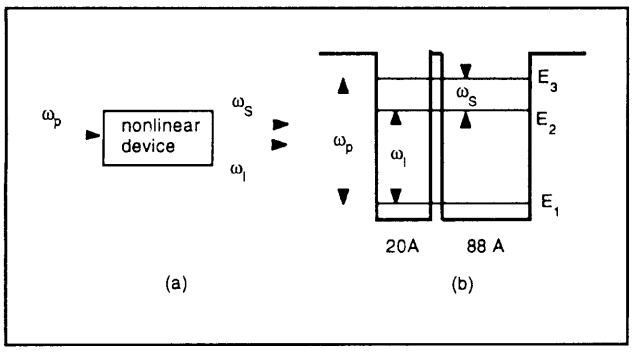

Figure 11. (a) Illustration of parametric amplification process, which converts a photon with a frequency ωP into two photons with frequencies ω_I and ω_S, with $\omega_I + \omega_S = \omega_P$. (b) An asymmetric DQW structure that could produce a large $\chi^{(2)}$ at mid- and far-infrared frequencies.

However, a single quantum well has inversion symmetry, and therefore has a vanishing $\chi^{(2)}$. This problem can be solved easily by using a coupled DQW structure with an asymmetric well widths, as shown in figure 11b. In this structure, the energy differences between level 3 and levels 1 and 2 are close to 120 meV (corresponding to a wavelength of 10 microns). These intersubband transition energies correspond to the pump and idler frequencies. The energy difference between levels 1 and 2 is approximately 20 meV, corresponding to the far-infrared signal frequency. The nonlinear susceptibility $\chi^{(2)}$ is proportional to the product of three dipole moments, $<Z_{12}><Z_{13}><Z_{23}>$. By careful design, each dipole moment can be as large as several tens of Å, which is at least one order of magnitude larger than that for optical transitions in atomic systems. Using the doubly resonant structure shown in figure 11(b), we estimate $\chi^{(2)}$ to be as large as 10^{-6} m/V, which is four orders of magnitude larger than the value for bulk GaAs materials. This extraordinarily large $\chi^{(2)}$ can be used for efficient parametric amplifications. The challenging issue of phase-matching can be solved by using Stark effect (changing the resonant conditions by applying a bias voltage) to diminish $\chi^{(2)}$ beyond the coherence length.

3.5 Millimeter-wave, THz, and Subpicosecond Facilities

Professor Hu's laboratory is equipped with various millimeter-wave and infrared sources which can generate coherent and incoherent radiation from 75 GHz up to 30 THz. These include: Gunn oscillators at W-band frequencies (75-11 GHz); a frequency doubler, tripler, and quadrupler using Schottky diodes at 200, 300, and 400 GHz; an optically pumped far-infrared laser which generates coherent radiation from 245 GHz to 8 THz; and a far-infrared and an infrared Fourier transform spectrometer which are capable in performing linear spectroscopy from 45 GHz to 300 THz and beyond. This laboratory is also equipped with various cryogenic millimeter-wave and infrared detectors. These include: a Ge:Ga photoconductive detector, Si composite bolometers, InSb hot-electron bolometers, SIS (superconductor-insulator-superconductor) receivers, and high-T_c Josephson detectors. Recently, with support from AT&T, a mode-locked Ti:Sapphire laser, that can generate optical pulses as short as 70 femtosecond, was purchased and installed.

3.6 Publications

de Lange, G., B.R. Jacobson, and Q. Hu. "A Low-noise Micromachined Millimeter-wave Heterodyne Mixer with Nb Superconducting Tunnel Junctions." *Appl. Phys. Lett.* 68: 1862 (1996).

Hu, Q., S. Verghese, R.A. Wyss, T. Schä, J. del Alamo, S. Feng, K. Yakubo, M.J. Rooks, M.R. Melloch, and A. Förster. "High-Frequency (f ~ 1 THz) Studies of Quantum-effect Devices." *Semiconduct. Sci. Tech.* 11: 1888 (1996).

Lyubomirsky, I., and Q. Hu. "Optical Parametric Oscillators Without Phasematching." *J. Opt. Soc. Amer. B.* Forthcoming.

Rahman, A., G. de Lange, and Q. Hu. "Micromachined Room-temperature Microbolometers for Millimeter-wave Detection." *Appl. Phys. Lett.* 68: 2020 (1996).

Smet, J.H., C.G. Fonstad, and Q. Hu. "Intrawell and Interwell Intersubband Transitions in Multiple Quantum Wells for Far-infrared Sources." *J. Appl. Phys.* 79: 9305 (1996).

Verghese, S., N. Zamdmer, E.R. Brown, A. Förster, and Q. Hu. "An Optical Correlator Using A Low-temperature-grown GaAs Photoconductor." *Appl. Phys. Lett.* 69: 842 (1996).

Verghese, S., N. Zamdmer, Q. Hu, and A. Förster. "Cryogenic Picosecond Sampling Using Fiber-coupled Photoconductive Switches." Submitted to *Appl. Phys. Lett.*

Yakubo, K., S. Feng, and Q. Hu. "Direct Simulation of Photon-assisted Quantum Transport." *Phys. Rev.* B 54: 7987 (1996).

Xu, B., and Q. Hu. "Grating Coupling for Intersubband Emission and Detection." *Appl. Phys. Lett.*, Forthcoming.

3.6.1 Conference Papers

de Lange, G., B.R. Jacobson, A. Rahman, E.K. Duerr, and Q. Hu. "Low-noise Micromachined SIS Mixers for Millimeter-wave Imaging Arrays." *Proceedings of the 7th International Symposium on Space Terahertz Technology*, Charlottesville, Virginia, March, 1996, pp 29-36.

de Lange, G., A. Rahman, E.K. Duerr, and Q. Hu. "Low-noise Micromachined SIS Mixers for Millimeter-wave Imaging Arrays." Paper presented at 1996 Applied Superconductivity Conference, Pittsburgh, Pennsylvania, August, 1996; *IEEE Trans. on Appl. Superconduct.* Forthcoming.

Hu, Q. "High-frequency (f ~ 1 THz) Studies of Quantum-effect Devices." IBM Research Center at Yorktown Heights, New York, April 29, 1996; MIT CMS colloquium, October 11, 1996; Department of Physics, Brown University, Providence, Rhode Island, October 17, 1996.

Hu, Q. "Terahertz Lasers Based on Intersubband Transition." Advanced Heterostructure Transistors Conference, Kona, Hawaii, December 1996.

Lyubomirsky, L., and Q. Hu. "Asymmetric Quantum Wells: A New Gain Medium for Optical Parametric Oscillators." Paper presented at 1996 Material Research Society Fall Meeting, Boston, Massachusetts, December, 1996.

Verghese, S., N. Zamdmer, Q. Hu, and A. Förster, "Fiber-coupled Photoconductive Sampling for Time-resolved Transport Measurements of Cryogenic Devices." Paper presented at the American Physical Society March meeting, St. Louis, Missouri *Bull. Amer. Phys. Soc.* 41: 660 (1996).

Xu, B., Q. Hu, and M.R. Melloch. "Intersubband Far-infrared Emission in Multiple Quantum Wells." Paper presented at Material Research Society Fall Meeting, Boston, Massachusetts, December 1996.

3.6.2 Patents Pending

Verghese, S., E.R. Brown, and Q. Hu. "Photonconductive Optical Correlator." (MIT Case No. 7119L).

3.6.3 Theses

Rahman, A. *Room-temperature Micromachined Microbolometers for W-band (75-110 GHz) Focal-plane Imaging Arrays.* Ph.D. diss., Dept. of Electr. Eng. and Comput. Sci., MIT, 1996.

Wyss, R.A. *Far-infrared Radiation Response of Antenna-coupled Quantum-effect Devices.* Ph.D. diss., Dept. of Electr. Eng. and Comput. Sci., MIT, 1996.